Impact of solvent electrostatic environment on molecular junctions probed via electrochemical impedance spectroscopy

Wanzhuo Shi[†$], Julia E. Greenwald[†$], Latha Venkataraman[†‡*]

[†]Department of Chemistry, Columbia University, New York, New York 10027, United States
[‡]Department of Applied Physics and Applied Mathematics, Columbia University, New York, New York 10027, United States

[$]W.S. and J.E.G. contributed equally to this paper

[*]Email: lv2117@columbia.edu

Abstract.

The electrostatic environment around nanoscale molecular junctions modulates charge transport; solvents alter this environment. Methods to directly probe solvent effects require correlating measurements of the local electrostatic environment with charge transport across the metal-molecule-metal junctions. Here, we measure the conductance and current-voltage characteristics of molecular wires using scanning tunneling microscope-break junction (STM-BJ) setup in two commonly used solvents. Our results show that the solvent environment induces shifts in molecular conductance, which we quantify, but more importantly we find that the solvent also impacts the magnitude of current rectification in molecular junctions. Using electrochemical impedance spectroscopy incorporated into STM-BJ setup, we measure the capacitance of the dipole layer formed at the metal-solvent interface and show that rectification can be correlated with solvent capacitance. These results provide a method of quantifying the impact of the solvent environment and a path towards improved environmental control of molecular devices.

Keywords: Single-molecule junctions; scanning tunneling microscope; molecular junction rectification; electrochemical impedance spectroscopy.

The scanning tunneling microscope-break junction (STM-BJ) technique provides a facile method of forming metal-molecule-metal junctions under ambient conditions.[1, 2] Significant progress has been made in understanding how the chemical structure of the molecule impacts electron transport across the junction.[3-6] While several works have shown the solvent environment may be used to modulate conductance,[7-12] direct measurements that relate solvent properties to those of molecular junctions is lacking. Solvent molecules impact the electrostatic environment surrounding junction via the formation of an interfacial dipole layer on the electrode surface, which shifts the electrode work function and molecular orbital energy levels.[12-15] More polarizable solvent molecules are expected to form stronger dipole layers. Solvent-induced shifts in conductance are thus attributed to changes in the interfacial environment that dictate how the frontier molecular orbitals align with the Fermi level, E_F, of the electrodes.[16-18] Additionally, the screening effect of the dipole layers on the electrode surface changes the electric potential spatial distribution and further alters the electrostatic environment. The symmetry of the electrostatic environment can be broken by simply using two electrodes with different shapes, such as a wire cut sharp to form the tip and a flat substrate. Thus solvent polarity can also tune the current rectification in symmetric single-molecule junctions through asymmetric electrostatic environment.[17] However, it is difficult to accurately integrate solvent effects into molecular junction calculations[19] because the methods used to model the junction with atomic-level detail do not incorporate the larger, many-body solvent system due to the computational rigor required. Thus, an experimental method capable of interrogating the local electrostatic environment *and* measuring transport across single-molecule junctions is needed to study solvent-induced conductance effects. Herein, we measure the conductance and current-voltage (I-V) characteristics of two symmetric molecules using the STM-BJ technique in two different non-polar solvents.

Through fitting the I-V data, we are able to quantify the shift in the molecular resonance position relative to the junction Fermi level induced by the solvent. By incorporating electrochemical impedance spectroscopy (EIS) into the STM-BJ, measured tip-solvent-substrate capacitance and show that trends in these capacitances correlate with the measured rectification observed in the IV curves.

We use a custom-built STM-BJ setup to measure the conductance and I-V curves of two molecules, 4,4''-Diamino-p-terphenyl (DAT) and 4,4'-Bipyridine (BP) in two non-polar organic solvents commonly used in STM-BJ experiments, 1,2,4-trichlorobenzene (TCB) and 1-bromonaphthalene (BN) (see Figure 1a for structures). A gold STM tip (cut wire) and gold-coated substrate serve as the two electrodes (Figure 1b). Molecular junctions are formed by repeatedly forming and breaking gold point-contacts between the STM tip and substrate in a solution of target molecules. The junction conductance ($G = I/V$) is measured as a function of the relative displacement using an applied bias of 100 mV. Molecules with aurophilic linkers may bridge the gap between the two electrodes during tip retraction, thereby forming molecular junctions. The volume of solution deposited on the substrate is large enough such that both the tip and substrate are in contact with the solvent throughout the entire process. The retraction process is repeated thousands of times and measurements are compiled into one-dimensional (1D) conductance histograms (Figure 1c, d) without data selection. The corresponding two-dimensional (2D) conductance-displacement histograms are shown in SI Figure 1.[1, 3]

For junctions formed with DAT, we find the conductance is higher in BN than TCB (Figure 1c). DAT conducts through the highest occupied molecular orbital (HOMO) and has linkers that bind through a donor-acceptor motif with charge donation into the gold.[20] We next measure BP, which also forms donor-acceptor bonds, and conducts via the lowest unoccupied molecular orbital

(LUMO).[21] For BP, we observe a lower conductance in BN than TCB (Figure 1d), i.e. the opposite of what is observed for DAT. It is worth noting that the conductance histogram of BP displays two peaks corresponding to two distinct binding geometries.[22] A greater solvent dependence is observed for the lower conducting peak, which corresponds to a vertical binding geometry with a steeper transmission function.[21] From these conductance measurements, we conclude that for both molecules the HOMO (LUMO) must be aligned closer to (further away from) E_F in BN than in TCB, consistent with prior results.[11-13]

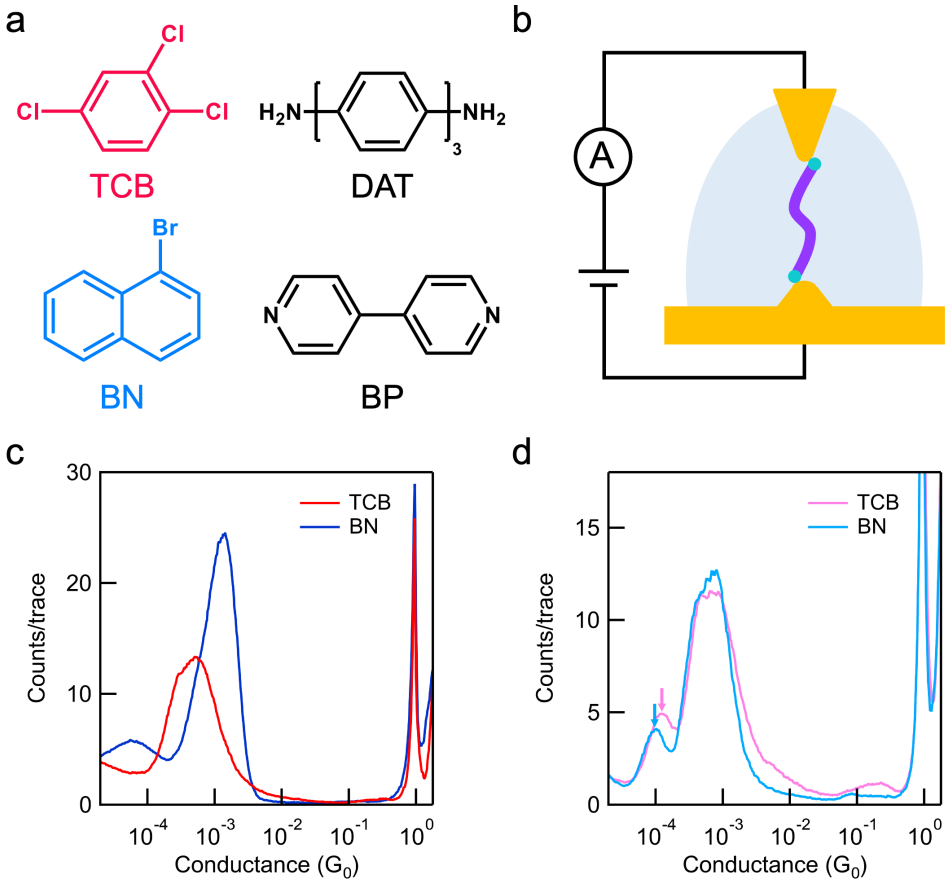

Figure 1. a) Structures of the two solvents studied, 1,2,4-trichlorobenzene (TCB, red) and 1-bromonaphthalene (BN, blue) and of the two molecules studied, 4,4"-Diamino-p-terphenyl (DAT) and 4,4'-Bipyridine (BP). b) Schematic of the custom STM-BJ setup showing a metal-molecule-metal junction. c) 1D conductance histograms for the HOMO conducting molecule DAT measured in TCB (red) and BN (dark blue). d) 1D conductance histograms for the LUMO conducting molecule BP measured in TCB (pink) and BN (light blue). The 1D conductance histograms are measured at 100 mV constructed from over 5,000 individual, consecutively measured traces.

We next modify the STM-BJ experiment to measure the current-voltage (I-V) properties of DAT and BP as follows: a bias of + 100 mV is applied as the tip is retracted from the substrate. After retracting the tip a fixed distance, the tip is held for 100 ms as the bias is swept between + 1 V and − 1 V. The tip is then further retracted at an applied bias of + 100 mV to break the junction. Two-dimensional I-V histograms are compiled from all traces that evidence a molecular junction and average IV curves (Figures 2a, b) are determined from the I-V histograms (SI Figure 2[23]).

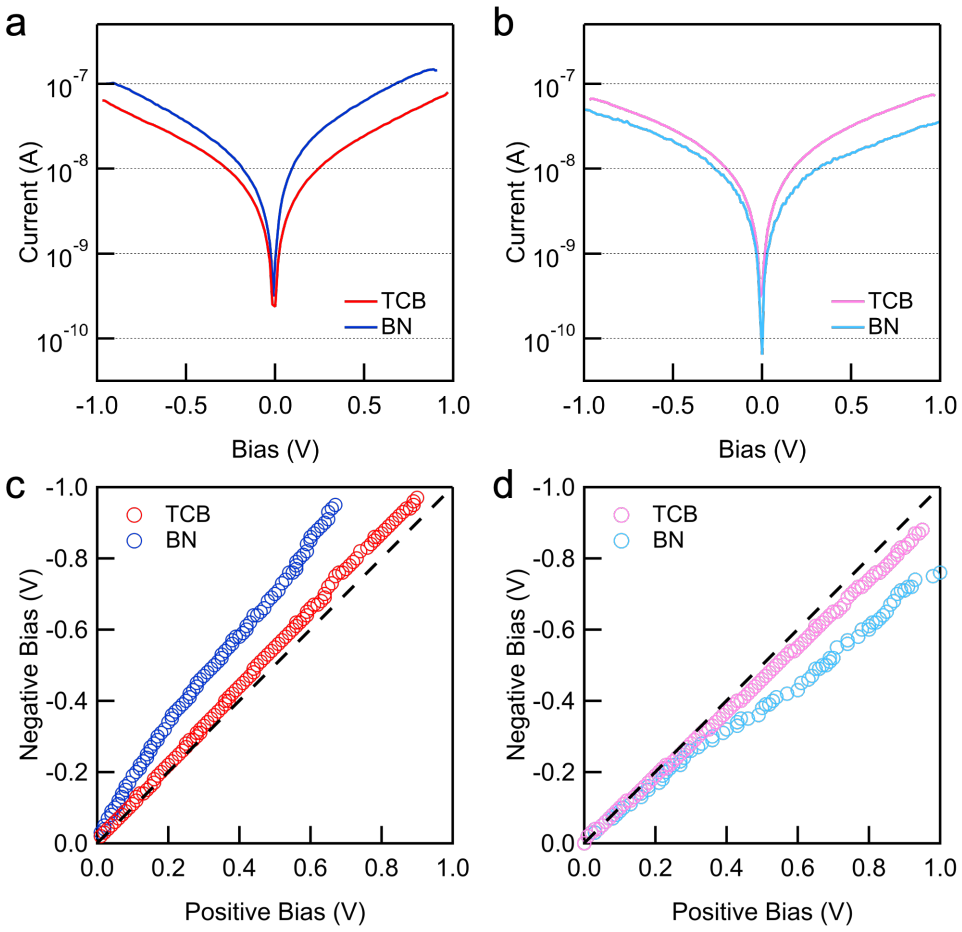

Figure 2. a) Average I-V curve for DAT measured in TCB (red) and BN (dark blue). b) Average I-V curve for BP measured in TCB (pink) and BN (light blue). Data obtained from 2D I-V histograms shown in SI Figure 2. c,d) Plots to quantify rectification of DAT in TCB (red) and BN (dark blue) and BP in TCB (pink) and BN (light blue). A perfectly symmetric I-V curve would lie

on the line x=y (dashed). The rectification plot for DAT falls above x=y, indicating a higher current is measured at positive bias than negative bias. The opposite effect is observed for BP.

Comparison of the average I-V curves in TCB and BN clearly demonstrates the impact of solvent on molecular junction current at both positive and negative applied biases. DAT (Figure 2a), a HOMO conductor, shows a lower current in TCB than BN at all biases. BP (Figure 2b), a LUMO conductor, shows the opposite trend, i.e., a lower current in BN than TCB at all biases. Together, the average I-V histograms for DAT and BP indicate that BN raises the electrostatic potential of the molecule (shifts the HOMO towards E_F) via surface interactions at all biases. These data are consistent with the 1D histograms shown in Figure 1 and highlight the impact of interfacial dipole layers on I-V characteristics.

Interestingly, both molecules exhibit rectification at high bias in BN and TCB. However, the magnitude of rectification is greater for junctions formed in BN. We quantify the magnitude and direction of rectification by separating the average I-V curves into two parts according to the bias polarity. The absolute values of the current in each part are compared and pairs of equal value are identified. These pairs are plotted as a scatter plot (Figure 2c, d) where the x and y coordinates correspond to the positive and negative bias values, respectively. A perfectly symmetric I-V curve would lie on the line $x = y$ (dashed). The rectification plot for DAT falls above $x = y$, indicating higher current is measured at positive biases. The reverse trend is observed for BP, i.e., the rectification plot falls below the line $x = y$ and a higher current is measured at negative biases. This is consistent with the fact that DAT is a HOMO conductor and BP is a LUMO conductor. Previous work in concentrated electrolytic environments has shown HOMO conductors have a higher current at positive tip bias while LUMO conductors have a higher current at negative tip bias. By restricting the exposed surface area on the tip side, the electric double layer density becomes significantly higher than on the substrate side. This strong local environmental

asymmetry induces a notable gating effect on the resonance position by the tip voltage, leading to opposite rectification effects for HOMO and LUMO conductors.[17]

We hypothesize the local electrostatic environment is different in TCB compared with BN, and to probe if these are indeed distinct, we measure the tip-solvent-substrate capacitance in both solvents using electrochemical impedance spectroscopy (EIS), a method which is commonly used to determine the capacitance of electric double layers.[24-26] In EIS experiments, impedance (Z) is measured as a function of frequency (ω). The resulting data is then fit to an equivalent electrochemical circuit where each circuit element describes a physical process occurring on a distinct timescale. Frequency-dependent measurements allow capacitive and resistive elements to be differentiated. The voltage and current flowing across a resistor are perfectly in-phase, whereas the current leads the voltage by 90° in a capacitor.

The same electronics and instrumentation are used for STM-BJ and STM-EIS measurements, which allows us to overcome sensitivity limits of commercial EIS instruments which typically cannot record sub-μA signals.[27,28-30] Specifically, we use the two-electrode EIS technique that does not rely on the use of a redox mediator.[31] An alternating bias is applied to the substrate ($V_{ac} = 25$ mV) on top of a dc bias ($V_{dc} = 100$ mV) and a current amplifier (Keithley 428) is used to measure the current at the tip. We form open junctions (see Figure 3a) by depositing a small volume (~ 10 μL) of pure solvent on the substrate and then hold the STM tip above the substrate at fixed displacement (~ 100 nm). A sample STM-EIS trace for TCB is shown in Figure 3b. The solvent nano-junction system is a linear system as confirmed by experiments detailed in SI Figure 3 and 4, allowing the application of the principle of superposition. Four discrete frequencies of equal magnitude are applied simultaneously to improve throughput. The voltage and current flowing across the open junction are measured in the time domain and converted to

the frequency domain via Fourier transform. For each applied frequency, the magnitude of impedance, $|Z|$, is calculated as follows

$$|Z(\omega)| = \frac{|V(\omega)|}{|I(\omega)|} \tag{1}$$

where $|V(\omega)|$ is the magnitude of the measured voltage at ω, ω is the angular frequency ($2\pi f$), and $|I(\omega)|$ is the magnitude of the measured current. The phase of impedance, θ, is calculated from the real and imaginary parts of Z as follows

$$\theta = \text{atan}\left(\frac{Im[Z(\omega)]}{Re[Z(\omega)]}\right). \tag{2}$$

The sample trace in Figure 3b shows that $|I|$ changes with the same applied $|V|$ at different frequencies, indicating the presence of a capacitive element in the equivalent electrochemical circuit for the open junction. The sample trace also highlights the sensitivity of the current amplifier, which enables us to measure extremely small (pA) currents.

To perform STM-EIS measurements on open junctions, multiple traces are collected as the applied frequency is varied across six orders of magnitude, from 0.1 Hz to 95 kHz. The magnitude and phase of impedance are then plotted versus frequency (Figures 3c, d) and fit to determine the equivalent electrochemical circuit. We find that for both solvents, the data can be fit with a parallel RC circuit, where R is the solution resistance and C is the interfacial capacitance at the tip-solvent-substrate junction. To determine exact values for R and C, we fit the magnitude of impedance versus frequency (Figure 3c) according to the equation for a parallel RC circuit:

$$\left|Z_{parallel}\right| = \frac{R}{\sqrt{1 + (\omega RC)^2}} \tag{3}$$

We find the solution resistance is higher in TCB (R_{TCB} = 36.6 GΩ) than BN (R_{BN} = 3.5 GΩ), while the junction capacitance is lower in TCB (C_{TCB} = 119 fF) than BN (C_{BN} = 153 fF). Note that we

have subtracted the intrinsic capacitance of the circuit components, such as coaxial cables, contribute to the overall capacitance from the value determined from the fit as these capacitances add to the circuit in parallel. The results of the EIS measurements for open junctions in air and additional measured examples in TCB and BN are presented in SI Figure 6. Using the resistance and capacitance values determined from fitting, we calculate the predicted phase according to the following equation,

$$\theta = \mathrm{atan}(-\omega RC) \tag{4}$$

We find that the predicted phase matches the measured phase for both solvents quite well (Figure 3d). We also evaluate a fitting method that includes both magnitude and phase information, as illustrated in Figure S5. The findings indicate that fitting based solely on magnitude is accurate, further confirming the open junctions can be described using a parallel RC circuit model.

The strength of the dipole layer at the interface is expected to scale with the measured capacitance.[32] The larger capacitance measured in BN than TCB, suggests a stronger dipole layer forms in BN than TCB. The ratio of the average measured capacitance between BN and TCB is $156.5\ \mathrm{fF} / 117.8\ \mathrm{fF} = 1.33$, which aligns with the ratios of other physical properties: dipole moment (BN: 1.93D, TCB: 1.40D, ratio: 1.38), polarizability (BN: 118.4 a. u., TCB: 90.6 a. u., ratio: 1.31), and permittivity (BN: 4.768 [33], TCB: 3.945 [34], ratio: 1.21). The dipole moments and polarizabilities are calculated, with detailed information provided in the SI. The small capacitance values measured in both TCB and BN (< 500 fF) demonstrate the sensitivity of the STM-EIS technique and the absence of the formation of a dense electric double layer in either solvent.

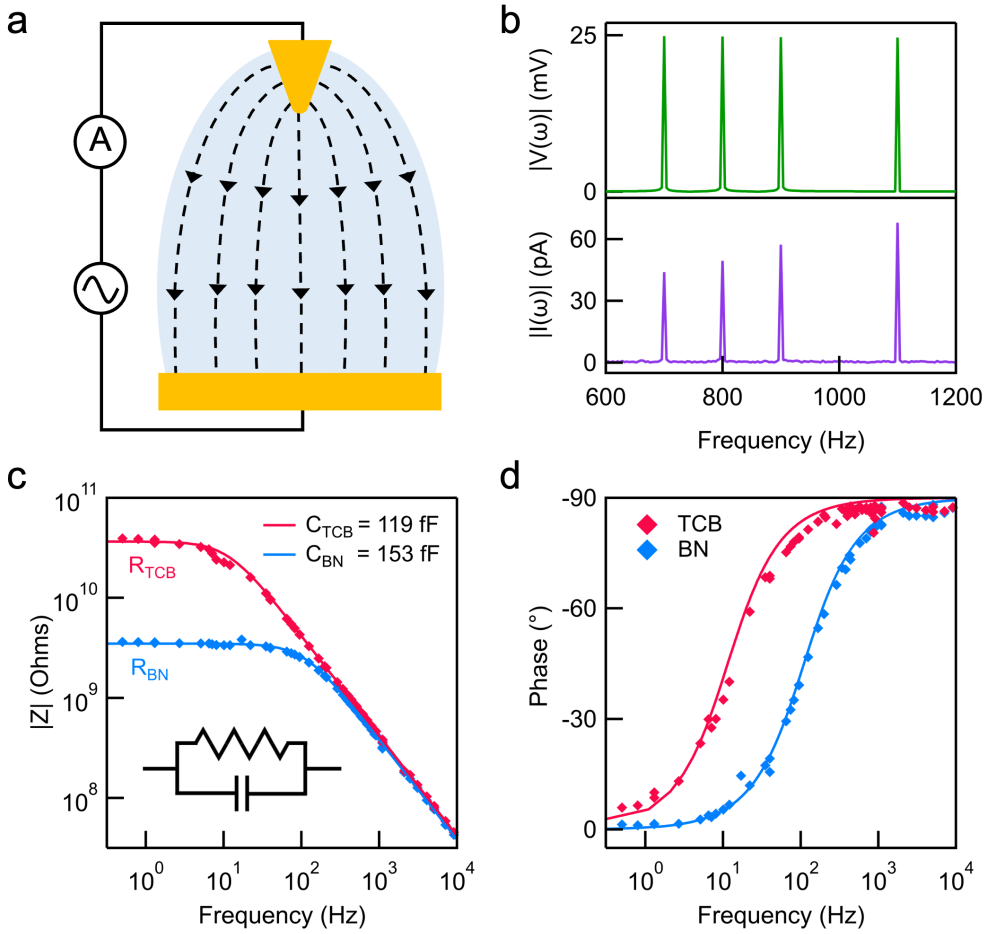

Figure 3. a) Schematic of the custom STM-EIS setup showing an open junction, where only solvent bridges the gap between the two electrodes b) Single STM-EIS trace showing the magnitude of the voltage (green, top) and current (purple, bottom) in the frequency domain. c) Magnitude and d) phase of impedance versus frequency for open junctions comprising pure solutions of TCB (red) and BN (blue). The open junctions may be described using a simple parallel RC circuit model (inset, c), where R_{sol} is the solution resistance and C_{sol} is the tip-solvent-substrate capacitance. The solid lines in c correspond to fitting the data to eq. 3. The solid lines in d are calculated according to eq. 4, using the values found from the fitting in c.

The higher capacitance measured in BN than TCB suggests the formation of a denser dipole layer at the metal-solvent interface, which means a stronger screening effect. Although the tip and substrate are typically assumed to be symmetric at the nanometer scale, they are asymmetric at the micron scale since the substrate is a large flat disc while the tip is a sharply cut wire. This leads to an asymmetry in the field distribution as illustrated in Figure 3a. A denser dipole layer

will accumulate at the tip, resulting in a non-linear electric potential drop across the nanojunction. As a result, the molecular junction is slightly gated by the tip bias which results in current rectification. We stress that the dipole layer at the interface must be quite diffused as an uncoated tip may be used in all experiments without the need to suppress any background capacitive or Faradaic currents.

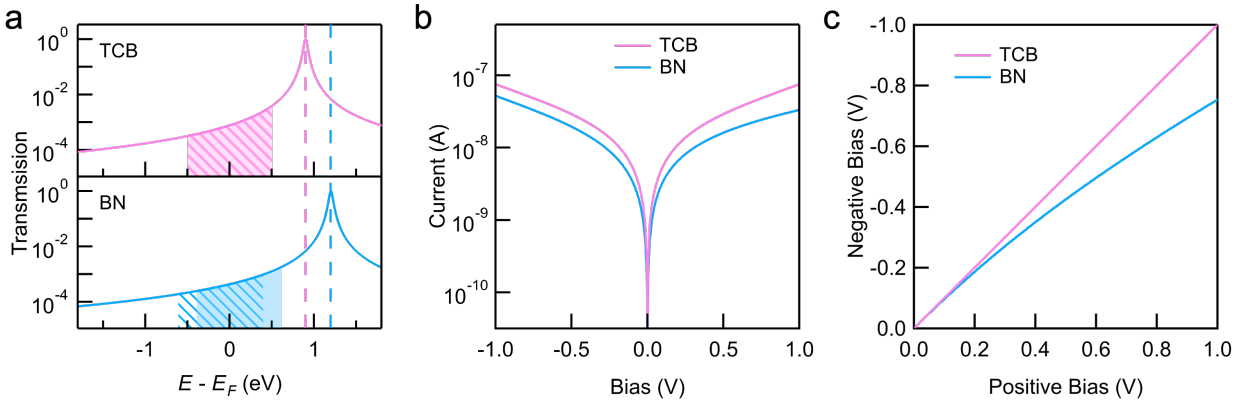

Figure 4. a) Transmission functions for BP fit using a single-level model (eq. 5). The resonance energy, ε, is found to be 0.95 eV for TCB (top) and 1.2 eV for BN (bottom). The coupling strength, i.e., resonance peak broadening in transmission, is the same in both solvents (Γ = 0.025 eV). The energy window is assumed to open symmetrically ($\alpha = 0$) in TCB and asymmetrically ($\alpha = 0.11$) in BN. The "line shade" and "solid shade" represent the energy windows under positive and negative bias, respectively. b) I-V curve for BP calculated in TCB (pink) and BN (light blue) using transmission functions from a. c) Rectification plots for BP in TCB (pink) and BN (light blue) calculated from I-V curves in b.

To provide a microscopic explanation of how the dipole layers affect molecular junction rectification, we model the energy dependence of transmission for a BP junction as a single-Lorentzian function, which has been shown to be accurate in past work.[21, 35]

$$T(E) = \frac{\Gamma^2}{(E-\varepsilon)^2 + \Gamma^2} \tag{5}$$

Here, ε is the orbital energy relative to E_F, Γ is the coupling of the orbital to the leads and T is the transmission. For BP, ε corresponds to the energy of the LUMO. Model transmission functions for BP in TCB and BN are shown in Figure 4a. We used the Landauer expression to obtain the current across the junction in the off-resonant coherent tunneling regime.[35, 36]

$$I(V) = \frac{2e}{h}\int_{-\infty}^{\infty} T(E)[f_S(E-\mu_S) - f_T(E-\mu_T)]dE \quad (6)$$

Here, e is the fundamental unit of charge, h is Planck's constant, V is the applied voltage bias across the junction, and $f_{S,T}(E-\mu_{S,T}) = 1/[1+\exp((E-\mu_{S,T})/k_BT)]$ are the Fermi-Dirac distributions of the substrate and tip electrodes, where k_BT is the thermal energy and $\mu_{S,T}$ are the electrochemical potentials of the tip and substrate, By applying a voltage across the tip and substrate, the energy window opens by $\mu_S - \mu_T = eV$ which drives current flow. When the potential drop across the junction is symmetric, $\mu_{S,T} = E_F \pm \frac{eV}{2}$, therefore no current rectification will be observed. However, when the voltage drops on two electrodes asymmetrically, the electrochemical potentials can be modified as $\mu_{S,T} = E_F \pm \frac{eV}{2} - \alpha eV$. The parameter α describes the asymmetry in the potential drop across the junction.[17] When α is 0.5, the local electrostatic environment is in an extreme condition in which the voltage drop is entirely confined at the tip contact. In this scenario, the potential at the tip is $\mu_T = E_F - eV$ and the electrochemical potential of the substrate is $\mu_S = E_F$. The substrate potential does not change in response to the bias applied to the tip because of strong screening effects at the tip. This is typically the case in highly polar solvents such as propylene carbonate, where a dense electric double layer forms around at the tip. However, as we will show below, small changes in α can be observed in non-polar solvents.

We fit the I-V curves shown in Figure 2b according to a single-level Landauer model (eq. 5, 6) to determine ε, the location of the BP resonance relative to E_F in each solvent. The LUMO resonance (dashed lines in Figure 4a) is found to be at 0.95 eV from E_F in TCB and 1.2 eV from E_F in BN, quantifying the impact of the solvent on level alignment. The coupling in both solvents is assumed to be the same and is determined from the fit to the I-V in TCB. The shaded areas in Figure 4a (the integral) represent the current across the junction for an applied bias of 1 V,

according to eq. 6 (Note that Fermi-Dirac distribution is omitted in the figure for simplicity.) The higher LUMO energy in BN causes a lower transmission around E_F, resulting in decreased conductance and consistent with experimental results (Figures 1d and 2b). As for the bias-dependent asymmetry observed in BN, it can be modelled simply by involving a non-zero α parameter. The energy window opens symmetrically in TCB ($\alpha = 0$) and asymmetrically in BN ($\alpha = 0.11$, determined from the fit). The "striped" and "solid" shades correspond to the energy windows under positive and negative biases. Figure 4a shows that for a LUMO conductor, the current flowing across the junction will be higher at negative biases. For the same reason, HOMO conductors will exhibit higher current at positive biases, consistent with the experimental results observed for DAT (Figure 1c and 2a). The averaged I-V curve for the DAT molecule is not fitted because its transmission function cannot be simply approximated by a single-level model.[20]

We use the fit parameters obtained above to generate theoretical I-V curves for BP in TCB and BN (Figure 4b), which nicely match the experimental results (Figure 2b). Current flow across the BP junction is systematically greater in TCB than BN because the LUMO resonance is aligned closer to E_F in TCB. Additionally, rectification is only seen in BN, and not TCB, because α is non-zero in BN. The calculated theoretical rectification plots for BP in TCB and BN are shown in Figure 4c. As expected, since $\alpha = 0$, the rectification trace for TCB lies on $x = y$, while in BN, it is below the line because of its LUMO conducting nature. We did not employ a coated tip to significantly enhance the surface charge density and disrupt the electrostatic environment's asymmetry in the junction in BN, therefore the asymmetry parameter α is only 0.11, far from the extreme case of 0.5 seen in polar solvents.[17] Nonetheless, this is sufficient to enable the simultaneous detection of distinct capacitance and polarity dependencies, demonstrating the sensitivity of our STM-EIS technology.

We have shown that STM-EIS can be used to measure the capacitance of open junctions in BN and TCB. From conductance measurements of two molecules, we confirm that HOMO conductors have a higher conductance in BN than TCB as the HOMO lies closer to E_F in BN. LUMO conductors show the opposite trend. Through I-V measurements, we are able to determine that the LUMO shifts by 0.25 eV relative to E_F when changing solvents from BN to TCB. The I-V measurements also show greater rectification in BN than TCB, regardless of dominant transport channel. We attribute this to a solvent-induced dipole layer on the Au surface that is able to tune the electrostatic potential distribution across the junction. Standard dc-based STM-BJ experiments do not provide a means of quantifying the strength of the dipole layer at the metal-solvent interface in molecular junctions or the extent of the asymmetry in charge density at the tip and substrate interfaces. Thus, STM-EIS allows for improved understanding of how the solvent environment impacts electron transport at the nanoscale and a route to improved environmental control of molecular devices.

Supporting Information

Additional conductance data and STM-EIS data.

Author Contributions

W.S and J.E.G contributed equally.

Notes

The authors declare no competing financial interest.

Acknowledgements

W.S. is supported by the U.S.-Israel Binational Science Foundation Award 2020327. This research was supported in part by the National Science Foundation Award NSF DMR-2241180.

References:

(1) Xu, B. Q.; Tao, N. J. J., Measurement of single-molecule resistance by repeated formation of molecular junctions, *Science,* **2003,** 301, 1221-1223.

(2) Venkataraman, L.; Klare, J. E.; Tam, I. W.; Nuckolls, C.; Hybertsen, M. S.; Steigerwald, M. L., Single-Molecule Circuits with Well-Defined Molecular Conductance, *Nano Letters,* **2006,** 6, 458-462.

(3) Venkataraman, L.; Klare, J. E.; Nuckolls, C.; Hybertsen, M. S.; Steigerwald, M. L., Dependence of single-molecule junction conductance on molecular conformation, *Nature,* **2006,** 442, 904-907.

(4) Danilov, A.; Kubatkin, S.; Kafanov, S.; Hedegard, P.; Stuhr-Hansen, N.; Moth-Poulsen, K.; Bjornholm, T., Electronic transport in single molecule junctions: Control of the molecule-electrode coupling through intramolecular tunneling barriers, *Nano Letters,* **2008,** 8, 1-5.

(5) Prindle, C. R.; Shi, W. Z.; Li, L.; Jensen, J. D.; Laursen, B. W.; Steigerwald, M. L.; Nuckolls, C.; Venkataraman, L., Effective Gating in Single-Molecule Junctions through Fano Resonances, *Journal of the American Chemical Society,* **2024,** 146, 3646-3650.

(6) Su, T. A.; Neupane, M.; Steigerwald, M. L.; Venkataraman, L.; Nuckolls, C., Chemical principles of single-molecule electronics, *Nature Reviews Materials,* **2016,** 1, 16002.

(7) Luka-Guth, K., et al., Role of solvents in the electronic transport properties of single-molecule junctions, *Beilstein J Nanotechnol,* **2016,** 7, 1055-1067.

(8) Choi, B.; Capozzi, B.; Ahn, S.; Turkiewicz, A.; Lovat, G.; Nuckolls, C.; Steigerwald, M. L.; Venkataraman, L.; Roy, X., Solvent-dependent conductance decay constants in single cluster junctions, *Chemical Science,* **2016,** 7, 2701-2705.

(9) Milan, D. C., et al., Solvent Dependence of the Single Molecule Conductance of Oligoyne-Based Molecular Wires, *The Journal of Physical Chemistry C,* **2016,** 120, 15666-15674.

(10) Gunasekaran, S.; Hernangómez-Pérez, D.; Davydenko, I.; Marder, S.; Evers, F.; Venkataraman, L., Near Length-Independent Conductance in Polymethine Molecular Wires, *Nano Letters,* **2018,** 18, 6387-6391.

(11) Dalmieda, J.; Shi, W. Z.; Li, L.; Venkataraman, L., Solvent-Mediated Modulation of the Au-S Bond in Dithiol Molecular Junctions, *Nano Letters,* **2024,** 24, 703-707.

(12) Fatemi, V.; Kamenetska, M.; Neaton, J. B.; Venkataraman, L., Environmental Control of Single-Molecule Junction Transport, *Nano Letters,* **2011,** 11, 1988-1992.

(13) Kotiuga, M.; Darancet, P.; Arroyo, C. R.; Venkataraman, L.; Neaton, J. B., Adsorption-Induced Solvent-Based Electrostatic Gating of Charge Transport through Molecular Junctions, *Nano Letters,* **2015,** 15, 4498-503.

(14) Heimel, G.; Romaner, L.; Zojer, E.; Bredas, J.-L., The Interface Energetics of Self-Assembled Monolayers on Metals, *Accounts of Chemical Research,* **2008,** 41, 721-729.

(15) Gehring, P.; Thijssen, J. M.; van der Zant, H. S., Single-molecule quantum-transport phenomena in break junctions, *Nature Reviews Physics,* **2019,** 1, 381-396.

(16) Capozzi, B.; Chen, Q.; Darancet, P.; Kotiuga, M.; Buzzeo, M.; Neaton, J. B.; Nuckolls, C.; Venkataraman, L., Tunable Charge Transport in Single-Molecule Junctions via Electrolytic Gating, *Nano Letters,* **2014,** 14, 1400-1404.

(17) Capozzi, B.; Xia, J.; Adak, O.; Dell, E. J.; Liu, Z.-F.; Taylor, J. C.; Neaton, J. B.; Campos, L. M.; Venkataraman, L., Single-molecule diodes with high rectification ratios through environmental control, *Nature Nanotechnology,* **2015,** 10, 522-527.

(18) Fung, E. D., et al., Breaking Down Resonance: Nonlinear Transport and the Breakdown of Coherent Tunneling Models in Single Molecule Junctions, *Nano Letters,* **2019,** 19, 2555-2561.

(19) Guédon, C. M.; Valkenier, H.; Markussen, T.; Thygesen, K. S.; Hummelen, J. C.; van der Molen, S. J., Observation of quantum interference in molecular charge transport, *Nature Nanotechnology,* **2012,** 7, 305-309.

(20) Quek, S. Y.; Venkataraman, L.; Choi, H. J.; Louie, S. G.; Hybertsen, M. S.; Neaton, J. B., Amine-gold linked single-molecule circuits: Experiment and theory, *Nano Letters,* **2007,** 7, 3477-3482.

(21) Kim, T.; Darancet, P.; Widawsky, J. R.; Kotiuga, M.; Quek, S. Y.; Neaton, J. B.; Venkataraman, L., Determination of Energy Level Alignment and Coupling Strength in 4,4′ -Bipyridine Single-Molecule Junctions, *Nano Letters,* **2014,** 14, 794-798.

(22) Quek, S. Y.; Kamenetska, M.; Steigerwald, M. L.; Choi, H. J.; Louie, S. G.; Hybertsen, M. S.; Neaton, J. B.; Venkataraman, L., Mechanically Controlled Binary Conductance Switching of a Single-Molecule Junction, *Nature Nanotechnology,* **2009,** 4, 230-234.

(23) Widawsky, J. R.; Kamenetska, M.; Klare, J.; Nuckolls, C.; Steigerwald, M. L.; Hybertsen, M. S.; Venkataraman, L., Measurement of voltage-dependent electronic transport across amine-linked single-molecular-wire junctions, *Nanotechnology,* **2009,** 20, 434009.

(24) von Hauff, E., Impedance Spectroscopy for Emerging Photovoltaics, *The Journal of Physical Chemistry C,* **2019,** 123, 11329-11346.

(25) Amirudin, A.; Thierry, D., Application of electrochemical impedance spectroscopy to study the degradation of polymer-coated metals, *Prog Org Coat,* **1995,** 26, 1-28.

(26) Varshney, M.; Li, Y. B., Interdigitated array microelectrodes based impedance biosensors for detection of bacterial cells, *Biosens Bioelectron,* **2009,** 24, 2951-2960.

(27) WaveDriver 100 EIS Potentiostat. https://pineresearch.com/shop/potentiostats/wavedriver-series/wavedriver100-bundles/ (June 14),

(28) Quick Check of EIS System Performance. https://www.gamry.com/application-notes/EIS/quick-check-of-eis-system-performance/ (June 14),

(29) Zou, F.; Thierry, D.; Isaacs, H. S., A high-resolution probe for localized electrochemical impedance spectroscopy measurements, *J Electrochem Soc,* **1997,** 144, 1957-1965.

(30) O'Hayre, R.; Feng, G.; Nix, W. D.; Prinz, F. B., Quantitative impedance measurement using atomic force microscopy, *J Appl Phys,* **2004,** 96, 3540-3549.

(31) Shkirskiy, V.; Kang, M.; McPherson, I. J.; Bentley, C. L.; Wahab, O. J.; Daviddi, E.; Colburn, A. W.; Unwin, P. R., Electrochemical Impedance Measurements in Scanning Ion Conductance Microscopy, *Analytical Chemistry,* **2020,** 92, 12509-12517.

(32) Bard, A. J.; Faulkner, L. R., *Electrochemical methods : fundamentals and applications*. Wiley: New York, 2001; p xxi, 833 p.

(33) Haynes, W. M., *CRC handbook of chemistry and physics*. CRC press: 2016.

(34) Dreisbach, R. R.; American Chemical, S., *Physical properties of chemical compounds*. American Chemical Society: Washington, D.C, 1955; p 3 Vols. : tables.

(35) Datta, S., *Electronic transport in mesoscopic systems*. Cambridge University Press: Cambridge, UK ; New York, 1997.

(36) Zotti, L. A.; Kirchner, T.; Cuevas, J. C.; Pauly, F.; Huhn, T.; Scheer, E.; Erbe, A., Revealing the Role of Anchoring Groups in the Electrical Conduction Through Single-Molecule Junctions, *Small,* **2010,** 6, 1529-1535.

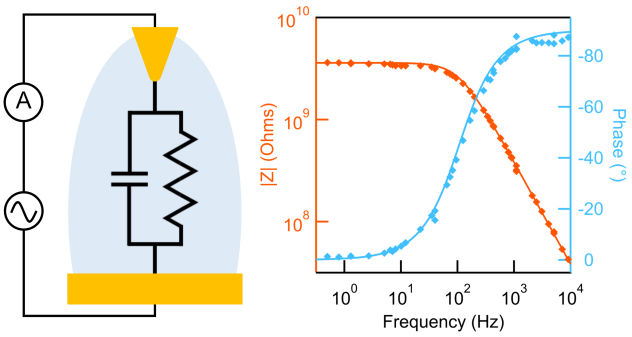
A
10^{10}
10^{9}
10^{8}
|Z| (Ohms)
-80
-60
-40
-20
0
Phase (°)
10^{0}
10^{1}
10^{2}
10^{3}
10^{4}
Frequency (Hz)